
POPGym Arcade: Parallel Pixelated POMDPs

Zekang Wang*

Faculty of Science and Technology
University of Macau
mc45154@um.edu.mo

Zhe He*

Faculty of Science and Technology
University of Macau
mc45189@um.edu.mo

Borong Zhang

Faculty of Science and Technology
University of Macau
mc45324@um.edu.mo

Edan Toledo

Department of Computer Science
University College London
ucabt01@ucl.ac.uk

Steven Morad[†]

Faculty of Science and Technology
University of Macau
smorad@um.edu.mo

Abstract

We present the POPGym Arcade³, a collection of hardware-accelerated, pixel-based environments with shared observation and action spaces. Each environment includes fully and partially observable variants, enabling counterfactual studies on partial observability. We also introduce mathematical tools for analyzing policies under partial observability, which reveal how agents recall past information to make decisions. Our analysis shows (1) that controlling for partial observability is critical and (2) that agents with long-term memory learn brittle policies that struggle to generalize. Finally, we demonstrate that recurrent policies can be “poisoned” by old, out-of-distribution observations, with implications for sim-to-real transfer, imitation learning, and offline reinforcement learning.

1 Introduction

Real-world decision making often requires reasoning under *partial observability*, where important information is hidden from the agent. This is a challenge for reinforcement learning (RL), which excels in fully observable settings (Silver et al., 2016). Scalable, efficient benchmarks for partial observability remain scarce, and existing solutions often lack tools to analyze how agents adapt to incomplete information.

Benchmarks like the Arcade Learning Environment (ALE) (Bellemare et al., 2013) and MuJoCo (Todorov et al., 2012) have driven RL progress, but they provide full or near-full observability (Machado et al., 2018), limiting their utility for partially observable scenarios. Prior work also rarely investigates *how* agents internally compensate for missing information over time.

We introduce POPGym Arcade (Fig. 1), a pixel-based, hardware-accelerated benchmark inspired by POPGym (Morad et al., 2023a) and the ALE. Each environment includes “twins”: fully and partially

*Equal Contribution

[†]Corresponding Author

³Code available at https://anonymous.4open.science/r/popgym_arcade-8F48/README.md

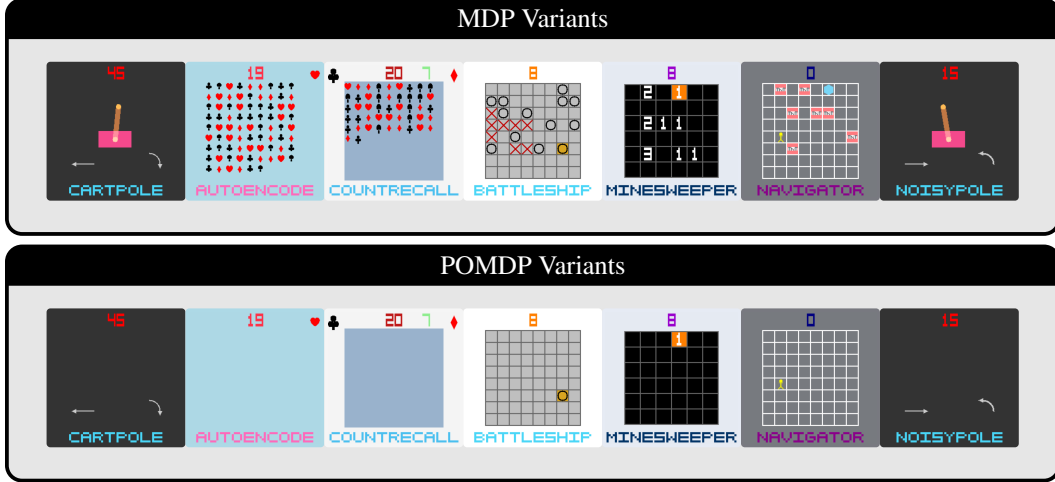


Figure 1: Observations from our environment twins. All environments share a unifying observation, state, and action space, enabling counterfactual studies with observability as the sole independent variable.

observable variants with identical dynamics, enabling controlled studies of observability. We complement this with tools to visualize how agents store and recall information, addressing the opacity of decision making under partial observability. By combining **hardware acceleration**, **environment twins**, and **pixel observations** with our **visualization tools**, we perform efficient counterfactual studies on observability, in a high-dimensional and interpretable observation space.

Contributions In this work, we contribute:

- GPU-accelerated, Atari-style partially observable environments.
- Fully observable twins for counterfactual studies on observability.
- Tools to examine how agents store and recall information over time.
- Evidence that solutions to partial observability introduce confounding factors.
- Evidence that recurrent value functions do not generalize well.

2 Background

In RL, we interact with an environment to maximize the discounted cumulative reward. A Markov Decision Process (MDP) (Sutton & Barto, 2018) is a tuple $\langle S, A, P, R, \gamma \rangle$, with the set of states S , actions A , and transition function $P : S \times A \mapsto \Delta(S)$, where $\Delta(S)$ is a distribution over S . MDPs also contain a reward function $R : S \times A \mapsto \mathbb{R}$ and discount factor $\gamma \in [0, 1]$. At each timestep, we receive a state $s_t \in S$ and select an action $a_t \in A$ from a policy $a_t \sim \pi(\cdot | s_t)$ that takes us to the next state following $P(s_{t+1} | s_t, a_t)$ while emitting a reward $r_t = R(s_t, a_t)$. We aim to learn the policy $\pi : S \mapsto \Delta(A)$ that maximizes the expected return $\mathbb{E}_\pi[\sum_{t=0}^{\infty} \gamma^t r_t | s_0 = s]$.

2.1 Partially Observable Markov Decision Processes

In many realistic scenarios, the agent does not have access to the full state of the environment, instead perceiving portions of the state through noisy or limited sensors. We call this problem setup a Partially Observable Markov Decision Process (POMDP). A POMDP is an extension of the MDP, consisting of tuple $\langle S, A, P, R, \gamma, \Omega, O \rangle$, with the set of observations Ω and the observation function $O : S \mapsto \Delta(\Omega)$. At each timestep, the agent can only access the current observation $o_t \sim O(s_t)$. The observation is not guaranteed to be Markov, thus providing only partial observability of the state, and preventing naive application of standard RL approaches to POMDPs. Fortunately, the sequence of all prior observations and actions, known as the trajectory $\mathbf{x}_t = (o_0, a_0, o_1, a_1 \dots a_{t-1}, o_t)$, is itself Markov (Sutton & Barto, 2018). As such, an optimal policy should consider all prior observations and actions.

2.2 Memory and Recurrences

For POMDPs, the optimal policy must be a function of a variable length trajectory \mathbf{x}_t . For conciseness, we introduce the combined observation-action space $X = (\Omega, A)$ and represent the observation and previous action as $x_t = (o_t, a_{t-1})$.

It is cumbersome to learn a policy over a variable size \mathbf{x}_t . We find it simpler to introduce a memory model f that produces a fixed-size latent Markov state $\hat{s} \in \hat{S}$ from the trajectory \mathbf{x}_t . This confines the complexities associated with partial observability to f , allowing the policy to operate on a latent Markov state \hat{s} . More formally, a recurrent memory model $f : X \times H \mapsto \hat{S} \times H$ maintains a summary of the trajectory in the recurrent state $h \in H$ and outputs a latent Markov state $\hat{s} \in \hat{S}$ for the policy

$$\hat{s}_t, h_t = f(x_t, h_{t-1}) \quad a_t \sim \pi(\cdot \mid \hat{s}_t). \quad (1)$$

Associative Recurrences Associative recurrent models, also known as linear recurrent models or memoroids (Morad et al., 2024), update the recurrent state with a binary operator \bullet that obeys the associative property

$$h_3 = (x_1 \bullet x_2) \bullet x_3 = x_1 \bullet (x_2 \bullet x_3). \quad (2)$$

Given an associative recurrent update, we can leverage the associative property to rearrange the order of operations. For example, given four inputs x_1, x_2, x_3, x_4 , we can compute either

$$h_4 = (((x_1 \bullet x_2) \bullet x_3) \bullet x_4) \quad h_4 = (x_1 \bullet x_2) \bullet (x_3 \bullet x_4). \quad (3)$$

The former case corresponds to standard recurrent networks, relying on the prior recurrent state to compute the current state, resulting in linear time complexity. In the latter case, we can compute $x_1 \bullet x_2$ and $x_3 \bullet x_4$ in parallel, achieving logarithmic parallel time complexity (Hinze, 2004). Blelloch (1990) provide an associative scan implementation with linear space complexity. Associative recurrences are orders of magnitude faster than classical RNNs in practice, while using much less memory than transformers, making them useful in sample inefficient tasks like RL (Lu et al., 2024).

Our experiments rely on four distinct associative recurrent models: the Fast Autoregressive Transformer (FART) (Katharopoulos et al., 2020), a form of State-Space Model (Gu et al., 2022) called the Linear Recurrent Unit (LRU) (Orvieto et al., 2023), and a GRU (Chung et al., 2014) variant of a Minimal Recurrent Network called the MinGRU (Feng et al., 2024). We provide formal descriptions of each model in Appendix H.

2.3 JAX and Hardware Acceleration

JAX (Bradbury et al., 2018) is a numerical computing library, supporting automatic differentiation, Just-In-Time (JIT) compilation, vectorization, and parallelization. JAX inspects python functions and translates them to XLA bytecode for hardware-specific JIT compilation. XLA compilation targets include CPUs, Tensor Processing Units (TPUs), GPUs and more. In RL, compiling the environment and algorithm together enables optimizations across the environment-agent interface.

3 Related Work

POMDP Benchmarks Progress in RL builds upon benchmarks that provide MDPs and POMDPs (Table 1). We specifically differentiate between weak POMDPs and strong POMDPs. **Weak POMDPs** admit near-optimal agents that consider just a few recent observations. Examples include Atari (Bellemare et al., 2013) which is known to be near-fully observable with framestacking (Machado et al., 2018), even for difficult games like Montezuma’s Revenge (Burda et al., 2022). Velocity-masked MuJoCo (Todorov et al., 2012; Ni et al., 2022) is another such weak POMDP (Morad et al., 2023a). We focus on **strong POMDPs**, where information is distributed over the trajectory such that long-term memory is necessary to achieve near-optimal returns. Examples of strong POMDPs include navigation tasks (Chevalier-Boisvert et al., 2018; Beattie et al., 2016; Kempka et al., 2016), psychological experiments (Fortunato et al., 2019), and memory games (Pleines et al., 2022; Morad et al., 2023a). Unfortunately, the cost of training memory models combined with the sample inefficiency of RL is prohibitively expensive, forcing researchers into a tradeoff between simplistic low-dimensional observation spaces, and skimping on the number of experiments used to back their claims.

Hardware-Accelerated RL Copying environment data from CPU to GPU during rollouts is a major efficiency bottleneck in the training process (Lu et al., 2022). Using JAX, one can implement their environments directly on accelerator hardware, avoiding cpu-to-accelerator copies and training policies up to one thousand times faster (Lange, 2022; Koyamada et al., 2023; Matthews et al., 2024b). We highlight Matthews et al. (2024a); Pignatelli et al. (2024); Lu et al. (2024) which offer hardware-accelerated strong POMDPs.

With improved environment throughput, we can consider new training paradigms like Podracer (Hessel et al., 2021; Toledo, 2024). In this work, we focus on the PQN algorithm (Gallici et al., 2024), a simplified podracer version of Q learning. Unlike DQN (Mnih et al., 2015), PQN does not use target networks or replay buffers, and opts for an on-policy TD(λ) objective.

Analyzing Memory in RL Prior work often focuses on designing memory models that maximize the return, but disentangling memory efficacy from confounding factors requires controlled benchmarks. Performance gaps between memory models could stem from parameter count disparities (Hansen et al., 2023) or implicit inductive biases (Morad et al., 2023b), rather than the ability of a memory model to learn a latent Markov state. To isolate the impact of partial observability, fully observable experimental controls (MDP twins) are critical. They allow us to quantify **how well a memory model mitigates partial observability** with certainty. Without such controls, claims about memory performance remain speculative. Controls that span environments are rare in literature – masked MuJoCo (Ni et al., 2022), for example, does not use a unified observation and action space between environments, necessitating changes in model architecture and weakening the control. To date, we are only aware of two benchmarks that enable controlling for observability across environments (Pleines et al., 2022; Rajan et al., 2023), and neither utilize hardware acceleration.

By measuring the return, we indirectly measure the quality of the latent Markov state \hat{s} created by the memory model. However, few works directly answer *how* the model constructs this latent state, providing hints but never complete answers. Hausknecht & Stone (2015); Kapturowski et al. (2019) measure how memory models function with stale recurrent states, while Morad et al. (2024) suggest that recurrent value functions may not operate as intended. Ni et al. (2024) decouples memory performance from temporal credit assignment, more directly measuring the quality of \hat{s} . Finally, (Elelimy et al., 2024; Morad et al., 2023b) examine the distribution of recurrent states. There is a gap in understanding concerning the meaning or source of memory contents.

4 Approach

In this section, we propose POPGym Arcade and derive tools for memory visualization.

4.1 Environments

POPGym Arcade consists of seven base environments (Appendix E), with a total of 84 environment configurations. Each environment has both small and large pixel observation spaces $\Omega_{\text{small}} = [0, 1]^{128 \times 128 \times 3}$, $\Omega_{\text{large}} = [0, 1]^{256 \times 256 \times 3}$. Similarly, all environments share the action space $A = \{\text{up, down, left, right, fire}\}$. We bound the undiscounted return for all environments in $[-1, 1]$ to simplify optimality gap and related comparisons. Finally, we implement three distinct difficulties for each environment.

Partially and Fully Observable Twins In our framework, MDP and POMDP environment twins share identical underlying state representations $s \in S$ transition dynamics $P(s_{t+1} | s_t, a_t)$, and observation spaces $o \in \Omega$, but exhibit distinct observation functions O . For the MDP variants, every observation o is guaranteed to be Markov, which is not true for the POMDP variants. We enforce an API boundary between P and O , which allows each environment to function as either a MDP or as a POMDP. A single shared observation and action space means we can use identical agent configurations for both POMDPs and MDPs. One can even change the observability or game itself mid-episode. With our POMDP-MDP twins, we execute studies with observability as the only independent variable. Model architecture, hyperparameters, and everything else can remain fixed.

Vectorized State Transitions and Rendering Given the poor sample efficiency of RL, we focus on maintaining high environment throughput. First and foremost, we ensure that all environ-

Table 1: Related benchmarks and their characteristics. A tilde in the MDP Twins columns means that MDP and POMDP twins do not share observation spaces, making causal studies difficult. Our benchmark is the only one with both strong POMDP/MDP twins and GPU acceleration.

Benchmark	Strong POMDPs	MDP Twins	Pixel Obs.	GPU
MuJoCo/MJX (Todorov et al., 2012)				✓
Atari/ALE (Bellemare et al., 2013)			✓	
DMLab (Beattie et al., 2016)	✓		✓	
VizDoom (Kempka et al., 2016)	✓		✓	
MiniGrid (Chevalier-Boisvert et al., 2018)	✓	~	✓	
Memory Task Suite (Fortunato et al., 2019)	✓		✓	
MinAtar (Young & Tian, 2019)			✓	
CuLE (Dalton & frosio, 2020)			✓	✓
EnvPool Weng et al. (2022)	✓		✓	✓
Gymnax (Lange, 2022)			✓	✓
POMDP Baselines (Ni et al., 2022)	✓	~		
MemoryGym (Pleines et al., 2022)	✓	✓	✓	
POPGym (Morad et al., 2023a)	✓	~		
PGX (Koyamada et al., 2023)				✓
MDP Playground (Rajan et al., 2023)	✓	✓	✓	
POPJaxRL (Lu et al., 2024)	✓			✓
Jumanji (Bonnet et al., 2024)	✓		✓	✓
Kinetix (Matthews et al., 2024b)			✓	✓
Craftax (Matthews et al., 2024a)	✓		✓	✓
Navix (Pignatelli et al., 2024)	✓	~	✓	✓
Brax/PixelBrax (Freeman et al., 2021; McInroe & Garcin, 2025)			✓	✓
POPGym Arcade (ours)	✓	✓	✓	✓

ments are both vectorizable and compilable to leverage hardware acceleration. Beyond this, we find a number of small tricks can improve performance. Pre-caching sprites and their pixel positions upon reset provides noticeable performance gains, and replacing calls to `jax.lax.cond` with `jax.lax.switch` provides increased throughput. See Appendix F for more information.

4.2 Memory Introspection Tools

With pixel observations, one can draw conclusions about how pixels impact value predictions (Greydanus et al., 2018). We implement visualization tools to probe which pixels the agent remembers, and their impact on the policy. More formally, given a trajectory \mathbf{x}_n , we compute latent Markov states $\hat{s}_0, \hat{s}_1, \dots, \hat{s}_n$ via Eq. (1). Then, we backpropagate through memory and policy, taking the absolute value of the gradient of Q values **with respect to an observation** o_t where $t \leq n$

$$\sum_{a_n \in A} |\nabla_{o_t} Q(\hat{s}_n, a_n)| = \sum_{a_n \in A} \left| \left(\frac{\partial}{\partial \hat{s}_n} Q(\hat{s}_n, a_n) \right) \frac{\partial \hat{s}_n}{\partial o_t} \right|, \quad (4)$$

where $|\cdot|$ denotes elementwise absolute value. This equation measures how much each pixel from a prior observation o_t propagates through memory and contributes to the Q values at time n . We derive a similar equation for policy gradient methods, instead measuring the impact on the action distribution

$$\int_A |\nabla_{o_t} \pi(a_n | \hat{s}_n)| da_n = \int_A \left| \left(\frac{\partial}{\partial \hat{s}_n} \pi(a_n | \hat{s}_n) \right) \frac{\partial \hat{s}_n}{\partial o_t} \right| da_n. \quad (5)$$

These methods produce qualitative saliency maps, describing pixel-level memory recall. We are also interested in a more quantitative and consistent measure, that elucidates the inner workings of memory in expectation over a distribution of trajectories. For these cases, we introduce the recall density, which we derive below.

Recall Density To achieve a more general notion of memory saliency, we start with Eqs. (4) and (5) and reduce over the observation dimensions using the L_1 norm, such that we receive a scalar

time-varying function z

$$z_Q(\mathbf{x}_n, t) = \sum_{a_n \in A} \|\nabla_{o_t} Q(\hat{s}_n, a_n)\|_1 \quad z_\pi(\mathbf{x}_n, t) = \int_A \|\nabla_{o_t} \pi(a_n | \hat{s}_n)\|_1 da_n, \quad (6)$$

where z_Q represents the quantity for Q functions and z_π for policies. Then, we normalize z , representing a scale-invariant density over trajectory \mathbf{x}_n

$$\delta_Q(\mathbf{x}_n, t) = \frac{z_Q(\mathbf{x}_n, t)}{\sum_{i=0}^n z_Q(\mathbf{x}_n, i)} \quad \delta_\pi(\mathbf{x}_n, t) = \frac{z_\pi(\mathbf{x}_n, t)}{\sum_{i=0}^n z_\pi(\mathbf{x}_n, i)}. \quad (7)$$

Finally, we take the sample mean over m trajectories to approximate the expected density under a policy π and memory model f

$$\frac{1}{m} \sum_{i=1}^m \delta_Q(\mathbf{x}_n^{(i)}, t) \approx \mathbb{E}_{\pi, f}[\delta_Q(\mathbf{x}_n, t)] \quad \frac{1}{m} \sum_{i=1}^m \delta_\pi(\mathbf{x}_n^{(i)}, t) \approx \mathbb{E}_{\pi, f}[\delta_\pi(\mathbf{x}_n, t)]. \quad (8)$$

We may compute the resulting expectation over all $0 \leq t \leq n$ to generate a plot summarizing memory recall.

Generalized Measures Thus far, n must be equal across all sampled trajectories, while in practice trajectories often differ in length. We use generalized time coordinates to resolve this issue. For each trajectory $\mathbf{x}^{(i)}$ of length n_i , we normalize the timestep $t \in \{0, \dots, n_i\}$ to a value $\tau = t/n_i \in [0, 1]$. We then compute the sample mean of the empirical densities at corresponding normalized time points across m trajectories

$$\frac{1}{m} \sum_{i=1}^m \delta_Q(\mathbf{x}_{n_i}^{(i)}, \lfloor \tau \cdot n_i \rfloor) \approx \mathbb{E}_{\pi, f}[\delta_Q(\mathbf{x}, \tau)] \quad \frac{1}{m} \sum_{i=1}^m \delta_\pi(\mathbf{x}_{n_i}^{(i)}, \lfloor \tau \cdot n_i \rfloor) \approx \mathbb{E}_{\pi, f}[\delta_\pi(\mathbf{x}, \tau)]. \quad (9)$$

We may compute the expectation over all $\tau \in [0, 1]$ to generate a plot summarizing memory recall. One should ensure that \mathbf{x} is not terminal, or risk evaluating Q or π at a terminal state.

Definition 4.1 (Recall Density). The Recall Density measures the expected relative influence of a past observation at the current timestep. For trajectories generated by policy π and memory model f , it quantifies how much an observation at normalized time $\tau \in [0, 1]$ impacts either:

- The Q value at trajectory end ($\mathbb{E}_{\pi, f}[\delta_Q(\mathbf{x}, \tau)]$), via Q gradient magnitudes
- The action distribution at trajectory end ($\mathbb{E}_{\pi, f}[\delta_\pi(\mathbf{x}, \tau)]$), via policy gradient magnitudes

Both variants normalize each observation’s influence by its trajectory’s total gradient magnitude, then average across trajectories. This handles variable-length trajectories by aligning timesteps to τ .

5 Experiments

Using our benchmark and visualization tools, we seek to answer three questions. See Appendices G and I for architecture and hyperparameter details.

How fast is POPGym Arcade? We leverage compilation and vectorization for improved throughput, but our large pixel observations take significant resources to render. In Fig. 2, we compare the throughput of our environments with Ω_{small} to other well-known environments over ten random seeds in Fig. 2, using an RTX4090 GPU and Intel I7 13700 CPU. We parallelize CPU environments using synchronous VectorEnvs, and shade the 95% bootstrapped confidence interval.

To what extent does memory mitigate partial observability? We execute a large scale study, training policies on all proposed environment, difficulty, and observability configurations over five random seeds. We evaluate three different associative recurrent backbones and an MLP backbone, and train the policy and backbones end-to-end using PQN. Using MDP performance as the control, we can measure exactly how well each memory architecture mitigates partial observability. We provide the full results in Appendix D, and aggregate results by model and observability in Fig. 3.

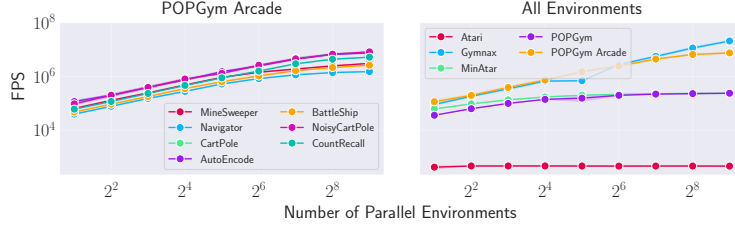


Figure 2: We plot the throughput of our environments in Frames Per Second (FPS), and compare to prior work. We achieve linear scaling with the number of environments, but saturate GPU cores and decay to sublinear scaling after 2^7 environments. Still, our method scales nearly as well as Gymnax, which uses small non-pixel observation spaces. POPGym Arcade is faster than Atari, and outperforms POPGym and MinAtar benchmarks while producing observations that are orders of magnitude larger.



Figure 3: We plot the normalized returns $\in [0, 1]$ over 5 seeds and all observability, memory model, and difficulty configurations for all environments. The boxes, line, and dot represent the quartiles, median, and mean respectively. We organize the results by observability and model for a counterfactual study of memory.

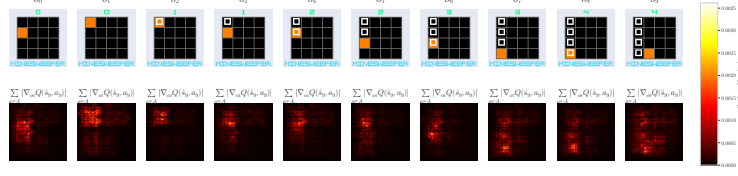
What role does memory play in RL? We investigate how our trained policies utilize memory. With pixel-space observations, we can visualize which pixels our agent recalls to make decisions. First, we use the memory analysis tools from Section 4.2 to inspect how individual memories qualitatively impact Q values (Fig. 4 and Appendix B). Then, we compute recall densities (Definition 4.1) over environment and model configurations to produce Appendix A. We aggregate densities across models into an environment summary in Fig. 5. Finally, we execute a toy experiment that introduces out-of-distribution observations into a recurrent policy, and investigate the results (Fig. 6 and Appendix C). In particular, we inject Gaussian noise $\mathcal{N}(0, 1)$ into an observation, and determine how this affects future Q values and actions for the LRU policy. Note that we generate a **fixed, noise-free trajectory** first using the trained policy. Only after do we inject noise into the trajectory, ensuring that the noise alone is responsible for changes in Q value.

6 Results

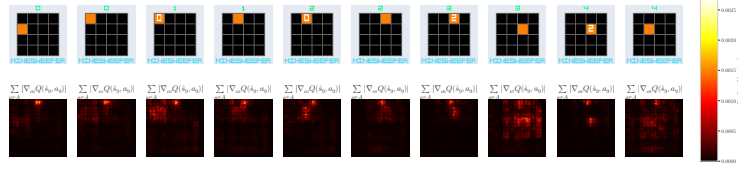
POPGym Arcade is fast. Our environments are faster than all CPU-based environments we tested (Fig. 2). For example, our observations are four orders of magnitude larger than POPGym, yet we run approximately two orders of magnitude faster. We achieve similar throughput to hardware-accelerated Gymnax while generating observations four orders of magnitude larger. One can quickly prototype models or algorithms on our pixel-space, partially observable tasks.

Memory models introduce confounding factors. There is a noticeable performance gap between memory models in our experiments (Fig. 3). The large gap between the POMDP and MDP control for the MLP demonstrates that memory is necessary to solve our benchmark.

Without confounding factors, all memory models should have the same MDP performance as the MLP, which is not the case. We initially suspected that the parameter increase associated with recurrent models would be a positive confounding factor, artificially boosting the final return compared to the MLP. The sizable gaps (MLP/MDP - FART/MDP) and (MLP/MDP - MinGRU/MDP) instead suggest large negative confounding factors – adding FART or MinGRU to a policy that does not



(a) Memory saliency map for the MineSweeper MDP.



(b) Memory saliency map for the MineSweeper POMDP.

Figure 4: How do our fully-trained agents use memory? We plot o_0, \dots, o_9 in the upper row. In the lower row, we plot pixel-wise recall (Eq. (4)) to compute $Q(\hat{s}_9, a_9)$ with respect to each observation. Surprisingly, LRU policies ignore the Markov property, relying on older observations instead. Note that our policy architecture utilizes a skip connection across the recurrent model, allowing the policy to bypass memory if not necessary.

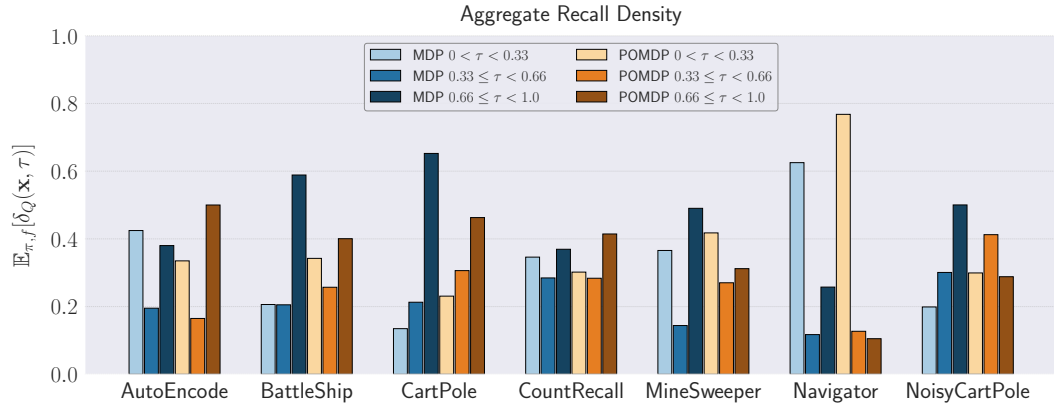


Figure 5: A quantitative inspection of memory. We use Definition 4.1 to estimate LRU recall density $\mathbb{E}_{\pi, f}[\delta_Q(\mathbf{x}, \tau)]$ for binned τ representing the start, middle, and end of a trajectory. We estimate the density using five trajectories per memory model, and aggregate over all memory models. The recall density tells us which observations the agent recalls for decision making. If memory models learned the Markov property (to ignore older observations), we would expect all MDP density to be in the $0.66 \leq \tau < 1.0$ bin. This is not what we see – in all cases, the distribution is spread throughout the full trajectory. Even for simple tasks like CartPole, the agent places considerable density on useless observations. Dependence on many prior observations suggests the policies may not generalize well.

need it is more likely to harm performance rather than help. Unlike the FART or MinGRU, the LRU appears to have marginal positive confounding factors (MLP/MDP - LRU/MDP). These findings cast doubt on prior work without control MDPs, emphasizing the importance of environment twins.

Recurrent policies ignore the Markov property. Figs. 4 and 5 and Appendices A and B all tell the same story – recurrent models tend to solve POMDPs and MDPs in the same manner, ignoring the Markov property. Even in fully observable tasks, recurrent models continue to rely on prior observations to predict Q values, even when such observations do not affect the return. We stress that all our recurrent policies include a residual connection that bypasses the memory model, allowing the agent to ignore prior observations if not necessary.

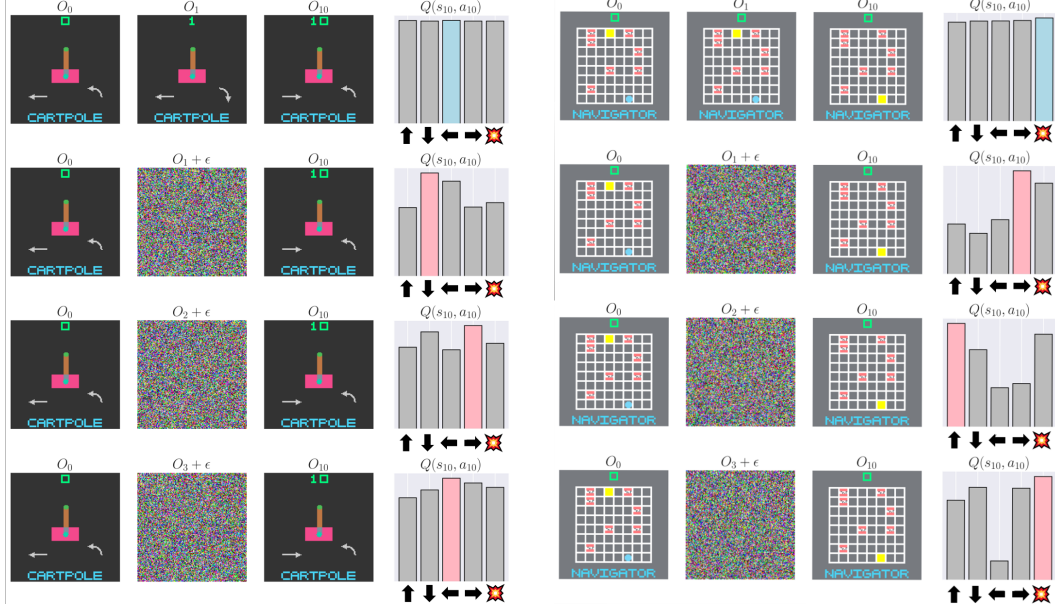


Figure 6: We can poison the recurrent state with out-of-distribution observations. First, we generate a trajectory following the greedy policy. Then, we inject noise ϵ into one selected observation, and examine how this information propagates into future actions. Note that each row follows an identical trajectory up to t , and noise is only present in one observation for each row. We see that not only does the future Q value change significantly, but so does the greedy action.

Out-of-distribution observations poison recurrent states. Recurrent policies rely on many unnecessary prior observations (Figs. 4 and 5). Therefore, out-of-distribution observations can “poison” the recurrent state, affecting Q values and agent decisions far into the future (Figs. 6 and 12). Both Q values and policy actions are sensitive to this phenomena. Demonstrating this on a simple task like CartPole does not bode well for more complex and realistic tasks. These results have far-reaching implications for offline RL, imitation learning, or sim-to-real scenarios, where we expect the agent to encounter out-of-distribution observations after training. A single out-of-distribution observation could poison the agent, altering its behavior long after the observation occurred.

6.1 Limitations and Future Work

Should we limit context? Recurrent models exhibit poor robustness due to reliance on many past observations. Unlike recurrent policies, a framestack or transformer policy may be harder to poison. They will discard the out-of-distribution observation when it exceeds the context window, returning to an in-distribution context.

Regularization may push parameters towards simpler policies that rely on fewer observations, but one must be careful combining standard regularization with recurrent models. For example, applying naive L_2 regularization could worsen the problem for the MinGRU, by minimizing W_1, b_1 in the forget gate and retaining observations for longer: $h_t = (1 - \sigma(W_1 x_t + b_1)) \odot h_t + \dots$. Recurrent dropout or similar methods may be better suited to the task.

Finally, our poisoning experiment is just a proof of concept, not a rigorous analysis. Non-toy problems have more complex observation models that could impact Q values differently.

Resource constraints POPGym Arcade rendering logic eventually saturates GPU cores given enough parallel environments, resulting in further environments exhibiting sublinear scaling (Fig. 2). More powerful GPUs should push this saturation point out further.

We have insufficient resources to perform proper grid searches for model-specific hyperparameters, given the number of environment configurations. Instead, we slightly modify the parameters from

the PQN paper to reduce the return variance between random seeds. Further tuning could improve the performance of various recurrent models.

7 Conclusion

We proposed POPGym Arcade, a collection of hardware-accelerated, pixel-based POMDPs, MDPs, and memory introspection tools. Using our library, we detected powerful confounding factors when evaluating memory models. We found that memory models use unnecessary information to build Markov states, with negative consequences for robustness.

References

- Andrew G. Barto, Richard S. Sutton, and Charles W. Anderson. Neuronlike adaptive elements that can solve difficult learning control problems. *IEEE Transactions on Systems, Man, and Cybernetics*, SMC-13(5):834–846, 1983. DOI: 10.1109/TSMC.1983.6313077.
- Charles Beattie, Joel Z. Leibo, Denis Teplyashin, Tom Ward, Marcus Wainwright, Heinrich Küttler, Andrew Lefrancq, Simon Green, Víctor Valdés, Amir Sadik, Julian Schrittwieser, Keith Anderson, Sarah York, Max Cant, Adam Cain, Adrian Bolton, Stephen Gaffney, Helen King, Demis Hassabis, Shane Legg, and Stig Petersen. DeepMind Lab. Technical Report arXiv:1612.03801, arXiv, December 2016. URL <http://arxiv.org/abs/1612.03801>. arXiv:1612.03801 [cs] type: article.
- M. G. Bellemare, Y. Naddaf, J. Veness, and M. Bowling. The Arcade Learning Environment: An Evaluation Platform for General Agents. *Journal of Artificial Intelligence Research*, 47:253–279, June 2013. ISSN 1076-9757. DOI: 10.1613/jair.3912. URL <https://www.jair.org/index.php/jair/article/view/10819>.
- Guy E Blelloch. Prefix Sums and Their Applications. Technical report, School of Computer Science, Carnegie Mellon University, November 1990.
- Clément Bonnet, Daniel Luo, Donal Byrne, Shikha Surana, Sasha Abramowitz, Paul Duckworth, Vincent Coyette, Laurence I. Midgley, Elshadai Tegegn, Tristan Kalloniatis, Omayma Mahjoub, Matthew Macfarlane, Andries P. Smit, Nathan Grinsztajn, Raphael Boige, Cemlyn N. Waters, Mohamed A. Mimouni, Ulrich A. Mbou Sob, Ruan de Kock, Siddarth Singh, Daniel Furelos-Blanco, Victor Le, Arnau Pretorius, and Alexandre Laterre. Jumanji: a Diverse Suite of Scalable Reinforcement Learning Environments in JAX, 2024. URL <https://arxiv.org/abs/2306.09884>. eprint: 2306.09884.
- James Bradbury, Roy Frostig, Peter Hawkins, Matthew James Johnson, Chris Leary, Dougal Maclaurin, George Necula, Adam Paszke, Jake VanderPlas, Skye Wanderman-Milne, and Qiao Zhang. JAX: composable transformations of Python+NumPy programs, 2018. URL <http://github.com/jax-ml/jax>.
- Greg Brockman, Vicki Cheung, Ludwig Pettersson, Jonas Schneider, John Schulman, Jie Tang, and Wojciech Zaremba. Openai gym, 2016.
- Yuri Burda, Harrison Edwards, Amos Storkey, and Oleg Klimov. Exploration by Random Network Distillation. February 2022. URL <https://openreview.net/forum?id=H1lJJnR5Ym>.
- Lili Chen, Kevin Lu, Aravind Rajeswaran, Kimin Lee, Aditya Grover, Misha Laskin, Pieter Abbeel, Aravind Srinivas, and Igor Mordatch. Decision Transformer: Reinforcement Learning Via Sequence Modeling. *Advances in neural information processing systems*, 34:15084–15097, 2021.
- Maxime Chevalier-Boisvert, Lucas Willems, and Suman Pal. Minimalistic Gridworld Environment for OpenAI Gym, 2018. URL <https://github.com/maximecb/gym-minigrid>. Publication Title: GitHub repository.
- Junyoung Chung, Caglar Gulcehre, Kyunghyun Cho, and Yoshua Bengio. Empirical evaluation of gated recurrent neural networks on sequence modeling. In *NIPS 2014 Workshop on Deep Learning, December 2014*, 2014.
- Steven Dalton and iuri frosio. Accelerating Reinforcement Learning through GPU Atari Emulation. In *Advances in Neural Information Processing Systems*, volume 33, pp. 19773–19782. Curran Associates, Inc., 2020. URL <https://proceedings.neurips.cc/paper/2020/hash/e4d78a6b4d93e1d79241f7b282fa3413-Abstract.html>.
- Esraa Elelimy, Adam White, Michael Bowling, and Martha White. Real-Time Recurrent Learning using Trace Units in Reinforcement Learning. November 2024. URL <https://openreview.net/forum?id=4UvMOnZMam¬eId=SpwUrmTQx1>.
- Leo Feng, Frederick Tung, Mohamed Osama Ahmed, Yoshua Bengio, and Hossein Hajimirsadeghi. Were RNNs All We Needed? October 2024. URL <https://openreview.net/forum?id=GrmFFxGnOR>.

- Meire Fortunato, Melissa Tan, Ryan Faulkner, Steven Hansen, Adrià Puigdomènech Badia, Gavin Buttimore, Charles Deck, Joel Z Leibo, and Charles Blundell. Generalization of Reinforcement Learners with Working and Episodic Memory. In *Advances in Neural Information Processing Systems*, pp. 12448–12457, 2019.
- C. Daniel Freeman, Erik Frey, Anton Raichuk, Sertan Girgin, Igor Mordatch, and Olivier Bachem. Brax – A Differentiable Physics Engine for Large Scale Rigid Body Simulation, June 2021. URL <http://arxiv.org/abs/2106.13281>. arXiv:2106.13281 [cs].
- Matteo Gallici, Mattie Fellows, Benjamin Ellis, Bartomeu Pou, Ivan Masmitja, Jakob Nicolaus Foerster, and Mario Martin. Simplifying Deep Temporal Difference Learning, October 2024. URL <http://arxiv.org/abs/2407.04811>. arXiv:2407.04811 [cs].
- Samuel Greydanus, Anurag Koul, Jonathan Dodge, and Alan Fern. Visualizing and Understanding Atari Agents. In *Proceedings of the 35th International Conference on Machine Learning*, pp. 1792–1801. PMLR, July 2018. URL <https://proceedings.mlr.press/v80/greydanus18a.html>. ISSN: 2640-3498.
- Albert Gu, Karan Goel, and Christopher Re. Efficiently Modeling Long Sequences with Structured State Spaces. March 2022. URL <https://openreview.net/forum?id=uYLFoz1v1AC>.
- Nicklas Hansen, Hao Su, and Xiaolong Wang. TD-MPC2: Scalable, Robust World Models for Continuous Control. October 2023. URL <https://openreview.net/forum?id=0xh5CstDJU>.
- Matthew Hausknecht and Peter Stone. Deep Recurrent Q-Learning for Partially Observable MDPs. In *2015 AAAI Fall Symposium Series*, September 2015. URL <https://www.aaai.org/ocs/index.php/FSS/FSS15/paper/view/11673>.
- Matteo Hessel, Manuel Kroiss, Aidan Clark, Iurii Kemaev, John Quan, Thomas Keck, Fabio Viola, and Hado van Hasselt. Podracer architectures for scalable Reinforcement Learning, April 2021. URL <http://arxiv.org/abs/2104.06272>. arXiv:2104.06272 [cs].
- Ralf Hinze. An Algebra of Scans. In *Mathematics of Program Construction: 7th International Conference, MPC 2004, Stirling, Scotland, UK, July 12-14, 2004. Proceedings 7*, pp. 186–210. Springer, 2004.
- Sepp Hochreiter and Jürgen Schmidhuber. Long Short-Term Memory. *Neural Computation*, 9(8):1735–1780, November 1997. ISSN 0899-7667. DOI: 10.1162/neco.1997.9.8.1735. URL <https://doi.org/10.1162/neco.1997.9.8.1735>.
- Steven Kapturowski, Georg Ostrovski, John Quan, Remi Munos, and Will Dabney. Recurrent Experience Replay in Distributed Reinforcement Learning. In *International conference on learning representations*, 2019.
- Angelos Katharopoulos, Apoorv Vyas, Nikolaos Pappas, and François Fleuret. Transformers are RNNs: Fast Autoregressive Transformers with Linear Attention. In *Proceedings of the 37th International Conference on Machine Learning*, pp. 5156–5165. PMLR, November 2020. URL <https://proceedings.mlr.press/v119/katharopoulos20a.html>. ISSN: 2640-3498.
- Michał Kempka, Marek Wydmuch, Grzegorz Runc, Jakub Toczek, and Wojciech Jaśkowski. ViZ-Doom: A Doom-based AI Research Platform for Visual Reinforcement Learning. In *IEEE Conference on Computational Intelligence and Games*, pp. 341–348, Santorini, Greece, September 2016. IEEE. URL <http://arxiv.org/abs/1605.02097>.
- Sotetsu Koyamada, Shinri Okano, Soichiro Nishimori, Yu Murata, Keigo Habara, Haruka Kita, and Shin Ishii. Pgx: Hardware-Accelerated Parallel Game Simulators for Reinforcement Learning. In *Advances in Neural Information Processing Systems*, volume 36, pp. 45716–45743, 2023.
- Robert Tjarko Lange. gymnax: A JAX-based Reinforcement Learning Environment Library, 2022. URL <http://github.com/RobertTLange/gymnax>.
- Chris Lu, Jakub Kuba, Alistair Letcher, Luke Metz, Christian Schroeder de Witt, and Jakob Foerster. Discovered Policy Optimisation. *Advances in Neural Information Processing Systems*, 35:16455–16468, December 2022. URL https://proceedings.neurips.cc/paper_files/paper/2022/hash/688c7a82e31653e7c256c6c29fd3b438-Abstract-Conference.html.

- Chris Lu, Yannick Schroecker, Albert Gu, Emilio Parisotto, Jakob Foerster, Satinder Singh, and Feryal Behbahani. Structured State Space Models for in-Context Reinforcement Learning. *Advances in Neural Information Processing Systems*, 36, 2024.
- Marlos C. Machado, Marc G. Bellemare, Erik Talvitie, Joel Veness, Matthew Hausknecht, and Michael Bowling. Revisiting the Arcade Learning Environment: Evaluation Protocols and Open Problems for General Agents. *Journal of Artificial Intelligence Research*, 61:523–562, March 2018. ISSN 1076-9757. DOI: 10.1613/jair.5699. URL <https://jair.org/index.php/jair/article/view/11182>.
- Michael Matthews, Michael Beukman, Benjamin Ellis, Mikayel Samvelyan, Matthew Thomas Jackson, Samuel Coward, and Jakob Nicolaus Foerster. Craftax: A Lightning-Fast Benchmark for Open-Ended Reinforcement Learning. June 2024a. URL <https://openreview.net/forum?id=hg4wXlrQCV>.
- Michael Matthews, Michael Beukman, Chris Lu, and Jakob Foerster. Kinetix: Investigating the Training of General Agents through Open-Ended Physics-Based Control Tasks, October 2024b. URL <http://arxiv.org/abs/2410.23208>. arXiv:2410.23208 [cs].
- Trevor McInroe and Samuel Garcin. PixelBrax: Learning Continuous Control from Pixels End-to-End on the GPU, January 2025. URL <http://arxiv.org/abs/2502.00021>. arXiv:2502.00021 [cs].
- Volodymyr Mnih, Koray Kavukcuoglu, David Silver, Andrei A Rusu, Joel Veness, Marc G Bellemare, Alex Graves, Martin Riedmiller, Andreas K Fidjeland, Georg Ostrovski, and others. Human-Level Control Through Deep Reinforcement Learning. *nature*, 518(7540):529–533, 2015. Publisher: Nature Publishing Group.
- Steven Morad, Ryan Kortvelesy, Matteo Bettini, Stephan Liwicki, and Amanda Prorok. POPGym: Benchmarking Partially Observable Reinforcement Learning. In *The Eleventh International Conference on Learning Representations*, 2023a. URL <https://openreview.net/forum?id=chDrutUTsOK>.
- Steven Morad, Ryan Kortvelesy, Stephan Liwicki, and Amanda Prorok. Reinforcement Learning with Fast and Forgetful Memory. *Advances in Neural Information Processing Systems*, 36:72008–72029, December 2023b. URL https://proceedings.neurips.cc/paper_files/paper/2023/hash/e3bf2f0f10774c474de22a12cb060e2c-Abstract-Conference.html.
- Steven Morad, Chris Lu, Ryan Kortvelesy, Stephan Liwicki, Jakob Nicolaus Foerster, and Amanda Prorok. Recurrent Reinforcement Learning with Memoroids. November 2024. URL <https://openreview.net/forum?id=nA4Q983a1v>.
- Tianwei Ni, Benjamin Eysenbach, and Ruslan Salakhutdinov. Recurrent Model-Free RL Can Be a Strong Baseline for Many POMDPs. In *Proceedings of the 39th International Conference on Machine Learning*, pp. 16691–16723. PMLR, June 2022. URL <https://proceedings.mlr.press/v162/ni22a.html>. ISSN: 2640-3498.
- Tianwei Ni, Michel Ma, Benjamin Eysenbach, and Pierre-Luc Bacon. When Do Transformers Shine in RL? Decoupling Memory from Credit Assignment. *Advances in Neural Information Processing Systems*, 36, 2024.
- Antonio Orvieto, Samuel L Smith, Albert Gu, Anushan Fernando, Caglar Gulcehre, Razvan Pascanu, and Soham De. Resurrecting Recurrent Neural Networks for Long Sequences. In *Proceedings of the 40th International Conference on Machine Learning, ICML’23*. JMLR.org, 2023. Place: Honolulu, Hawaii, USA.
- Eduardo Pignatelli, Jarek Liesen, Robert Tjarko Lange, Chris Lu, Pablo Samuel Castro, and Laura Toni. NAVIX: Scaling MiniGrid Environments with JAX, July 2024. URL <http://arxiv.org/abs/2407.19396>. arXiv:2407.19396 [cs].
- Marco Pleines, Matthias Pallasch, Frank Zimmer, and Mike Preuss. Memory Gym: Partially Observable Challenges to Memory-Based Agents. September 2022. URL <https://openreview.net/forum?id=jHc8dCx6DDr>.

- Raghu Rajan, Jessica Lizeth Borja Diaz, Suresh Guttikonda, Fabio Ferreira, André Biedenkapp, Jan Ole von Hartz, and Frank Hutter. MDP Playground: An Analysis and Debug Testbed for Reinforcement Learning. *Journal of Artificial Intelligence Research*, 77:821–890, July 2023. ISSN 1076-9757. DOI: 10.1613/jair.1.14314. URL <http://arxiv.org/abs/1909.07750>. arXiv:1909.07750 [cs].
- David Silver, Aja Huang, Chris J. Maddison, Arthur Guez, Laurent Sifre, George van den Driessche, Julian Schrittwieser, Ioannis Antonoglou, Veda Panneershelvam, Marc Lanctot, Sander Dieleman, Dominik Grewe, John Nham, Nal Kalchbrenner, Ilya Sutskever, Timothy Lillicrap, Madeleine Leach, Koray Kavukcuoglu, Thore Graepel, and Demis Hassabis. Mastering the game of Go with deep neural networks and tree search. *Nature*, 529(7587):484–489, January 2016. ISSN 1476-4687. DOI: 10.1038/nature16961. URL <https://www.nature.com/articles/nature16961>. Publisher: Nature Publishing Group.
- Richard S Sutton and Andrew G Barto. *Reinforcement Learning: An Introduction*. MIT press, 2018.
- Emanuel Todorov, Tom Erez, and Yuval Tassa. MuJoCo: A physics engine for model-based control. In *2012 IEEE/RSJ International Conference on Intelligent Robots and Systems*, pp. 5026–5033, October 2012. DOI: 10.1109/IROS.2012.6386109. URL https://ieeexplore.ieee.org/abstract/document/6386109?casa_token=1tMZ2sK7IroAAAAA:VhBdmpcQ2-7j2n2asoRU2q0ZtxjiI3gcLmbFZscPxjgIhe267hBtCSJr_y__QuoXuGvfuoW-. ISSN: 2153-0866.
- Edan Toledo. Stoix: Distributed Single-Agent Reinforcement Learning End-to-End in JAX, April 2024. URL <https://github.com/EdanToledo/Stoix>.
- Jiayi Weng, Min Lin, Shengyi Huang, Bo Liu, Denys Makoviichuk, Viktor Makoviychuk, Zichen Liu, Yufan Song, Ting Luo, Yukun Jiang, Zhongwen Xu, and Shuicheng Yan. EnvPool: A Highly Parallel Reinforcement Learning Environment Execution Engine. June 2022. URL <https://openreview.net/forum?id=BubxnHpuMbG>.
- Kenny Young and Tian Tian. MinAtar: An Atari-Inspired Testbed for Thorough and Reproducible Reinforcement Learning Experiments, June 2019. URL <http://arxiv.org/abs/1903.03176>. arXiv:1903.03176 [cs].

A Recall Density Model and Task Breakdown

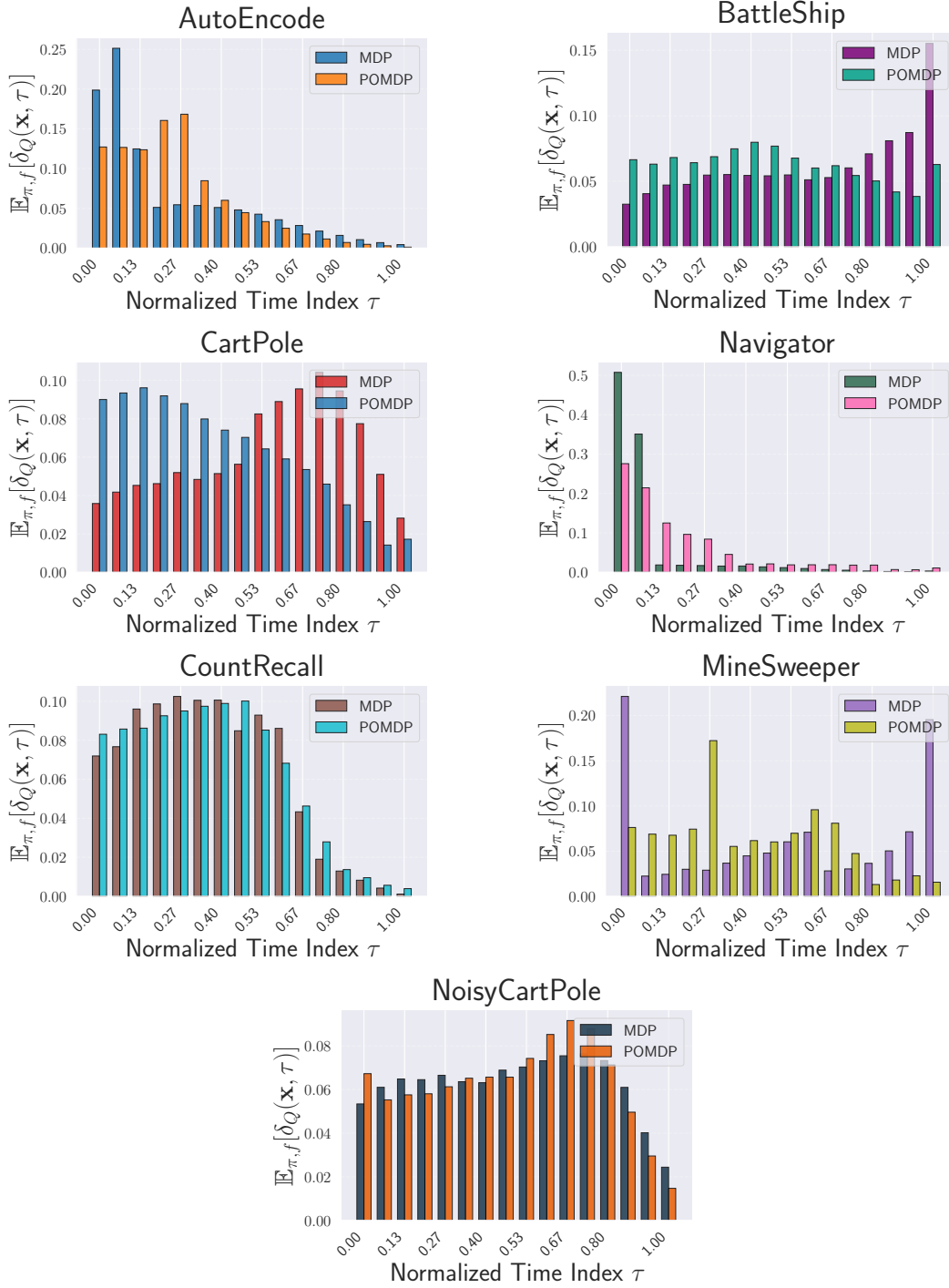


Figure 7: Recall density of FART categorized by environment, over five random seeds.

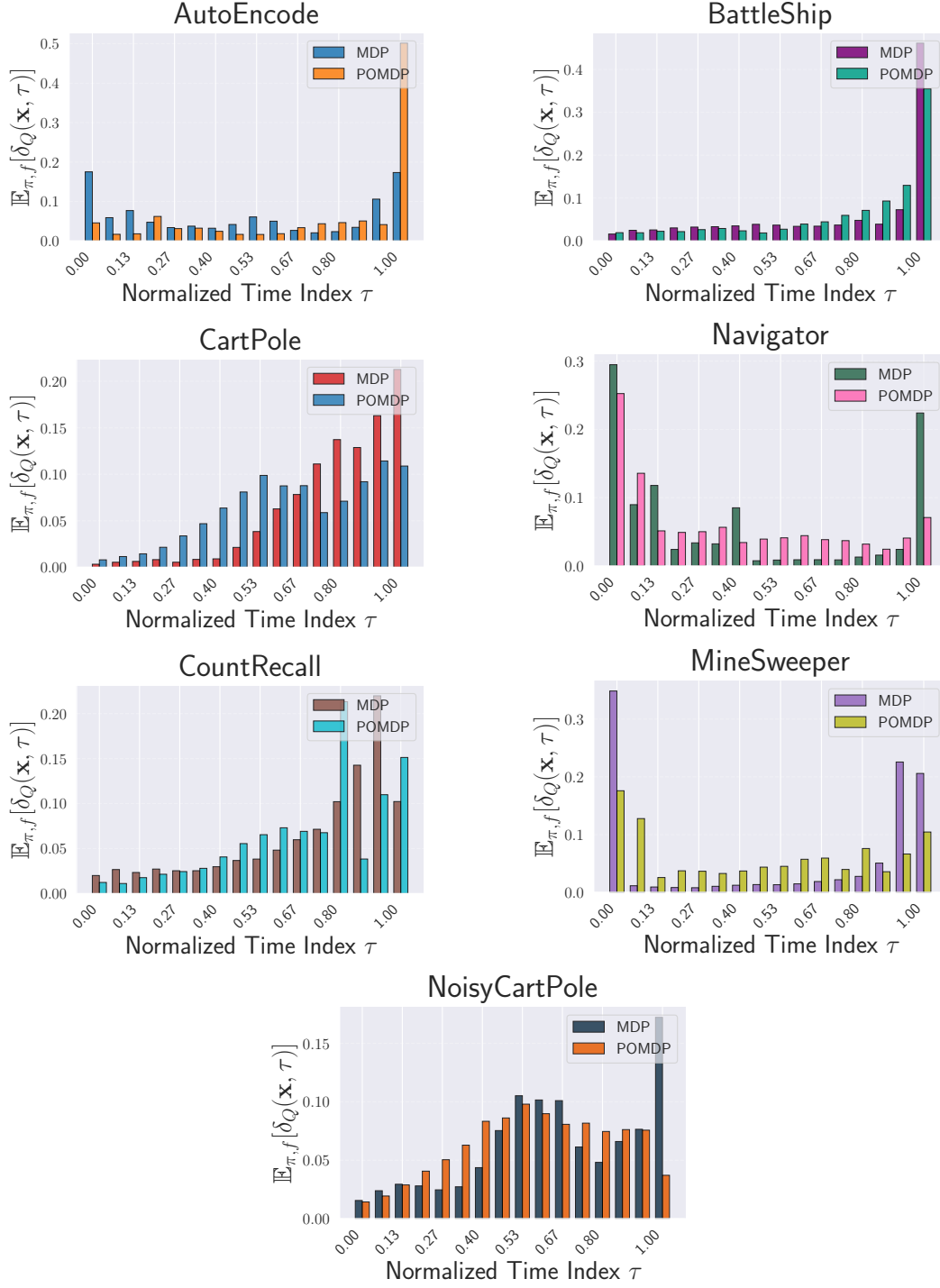


Figure 8: Recall density of LRU categorized by environment, over five random seeds.

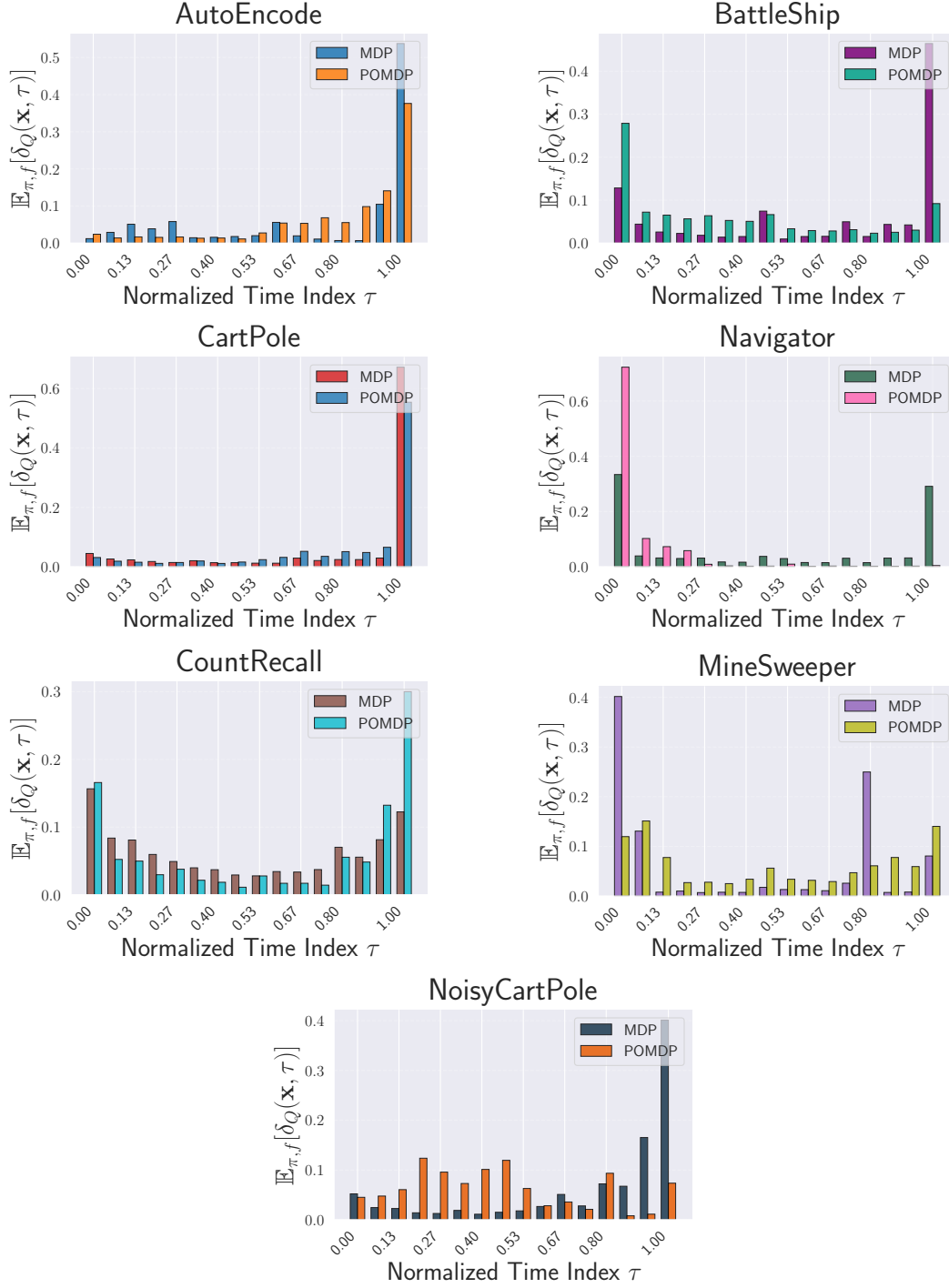
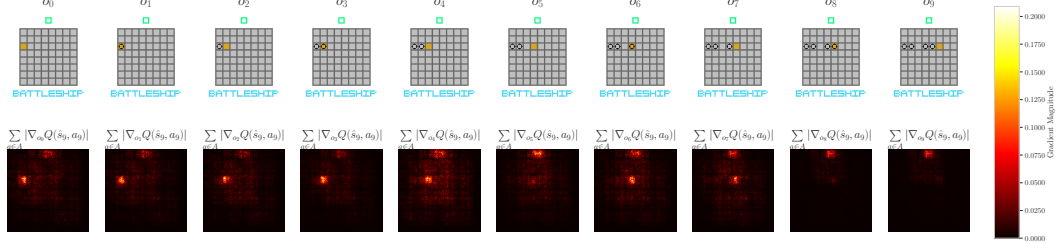
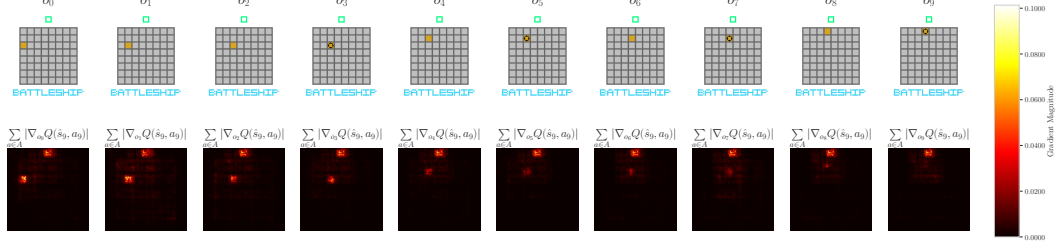


Figure 9: Recall density of MinGRU categorized by environment, over five random seeds.

B Additional Memory Analysis

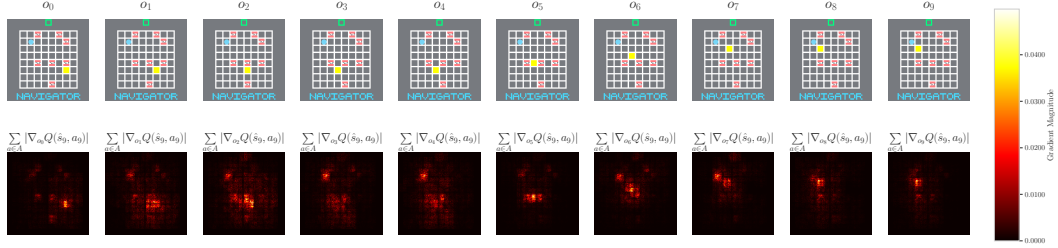


(a) Memory saliency map for the Battleship MDP

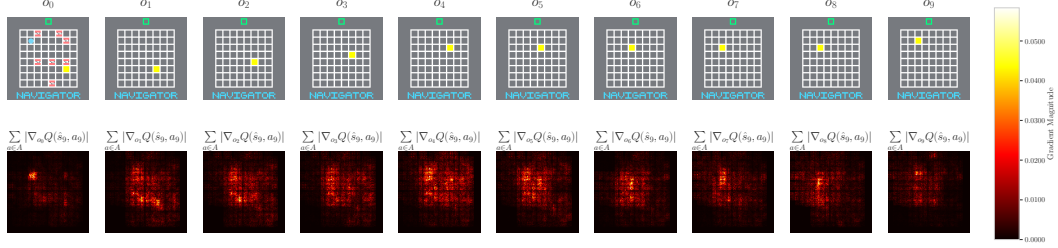


(b) Memory saliency map for the Battleship POMDP

Figure 10: LRU saliency plotted via Eq. (4).



(a) Memory saliency map for the Navigator MDP



(b) Memory saliency map for the Navigator POMDP

Figure 11: LRU saliency plotted via Eq. (4).

C Recurrent Policy Poisoning

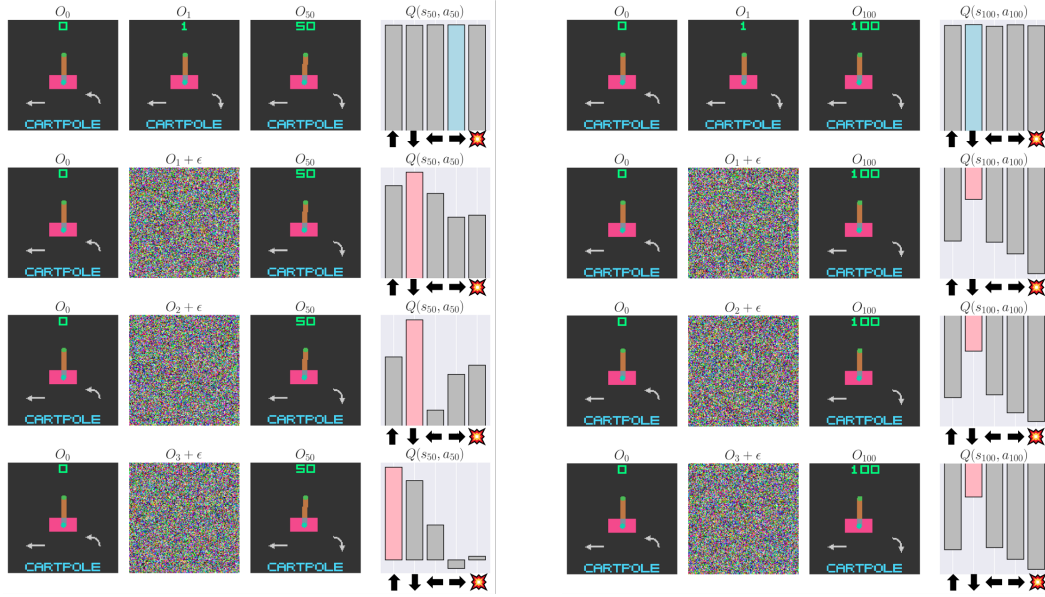


Figure 12: We demonstrate recurrent policy poisoning over longer horizons, using the LRU model. At 50 timesteps in the future, corrupted observations can still influence Q values enough to change the selected action. At 100 timesteps, adding noise results in negative Q values, but does not change the action in this specific case.

D Return Breakdown by Model

Table 2: Return for the LRU model, broken down by task and observability.

Environment	MDP Return	POMDP Return
AutoEncodeEasy	0.26 ± 0.00	0.27 ± 0.01
AutoEncodeMedium	0.24 ± 0.01	0.24 ± 0.00
AutoEncodeHard	0.23 ± 0.02	0.22 ± 0.02
BattleShipEasy	0.85 ± 0.02	0.84 ± 0.01
BattleShipMedium	0.78 ± 0.03	0.82 ± 0.01
BattleShipHard	0.73 ± 0.04	0.8 ± 0.01
CartPoleEasy	0.99 ± 0.00	0.99 ± 0.00
CartPoleMedium	0.98 ± 0.01	0.98 ± 0.01
CartPoleHard	0.97 ± 0.01	0.95 ± 0.02
CountRecallEasy	0.47 ± 0.06	0.36 ± 0.01
CountRecallMedium	0.22 ± 0.03	0.23 ± 0.04
CountRecallHard	0.15 ± 0.02	0.23 ± 0.01
MineSweeperEasy	0.87 ± 0.00	0.82 ± 0.01
MineSweeperMedium	0.67 ± 0.01	0.66 ± 0.01
MineSweeperHard	0.62 ± 0.01	0.61 ± 0.00
NavigatorEasy	0.91 ± 0.01	0.44 ± 0.09
NavigatorMedium	0.91 ± 0.01	0.32 ± 0.03
NavigatorHard	0.94 ± 0.01	0.4 ± 0.06
NoisyCartPoleEasy	0.99 ± 0.00	0.99 ± 0.00
NoisyCartPoleMedium	0.98 ± 0.01	0.99 ± 0.00
NoisyCartPoleHard	0.97 ± 0.01	0.97 ± 0.01

Table 3: Return for the MinGRU model, broken down by task and observability.

Environment	MDP Return	POMDP Return
AutoEncodeEasy	0.27 ± 0.00	0.27 ± 0.00
AutoEncodeMedium	0.25 ± 0.01	0.26 ± 0.00
AutoEncodeHard	0.25 ± 0.00	0.25 ± 0.00
BattleShipEasy	0.82 ± 0.02	0.76 ± 0.01
BattleShipMedium	0.73 ± 0.02	0.75 ± 0.02
BattleShipHard	0.71 ± 0.03	0.73 ± 0.02
CartPoleEasy	0.98 ± 0.01	0.87 ± 0.02
CartPoleMedium	0.93 ± 0.02	0.68 ± 0.06
CartPoleHard	0.88 ± 0.08	0.54 ± 0.03
CountRecallEasy	0.31 ± 0.01	0.29 ± 0.03
CountRecallMedium	0.17 ± 0.00	0.21 ± 0.04
CountRecallHard	0.15 ± 0.01	0.13 ± 0.04
MineSweeperEasy	0.83 ± 0.01	0.76 ± 0.01
MineSweeperMedium	0.64 ± 0.00	0.61 ± 0.00
MineSweeperHard	0.58 ± 0.01	0.58 ± 0.01
NavigatorEasy	0.89 ± 0.02	0.33 ± 0.08
NavigatorMedium	0.74 ± 0.08	0.25 ± 0.12
NavigatorHard	0.13 ± 0.45	0.08 ± 0.08
NoisyCartPoleEasy	0.95 ± 0.01	0.89 ± 0.01
NoisyCartPoleMedium	0.92 ± 0.01	0.86 ± 0.01
NoisyCartPoleHard	0.86 ± 0.02	0.81 ± 0.01

Table 4: Return for the FART model, broken down by task and observability.

Environment	MDP Return	POMDP Return
AutoEncodeEasy	0.25 ± 0.00	0.26 ± 0.00
AutoEncodeMedium	0.23 ± 0.01	0.23 ± 0.01
AutoEncodeHard	0.2 ± 0.03	0.21 ± 0.02
BattleShipEasy	0.66 ± 0.09	0.77 ± 0.02
BattleShipMedium	0.51 ± 0.01	0.52 ± 0.02
BattleShipHard	0.5 ± 0.00	0.5 ± 0.00
CartPoleEasy	0.98 ± 0.01	0.97 ± 0.01
CartPoleMedium	0.85 ± 0.06	0.78 ± 0.05
CartPoleHard	0.62 ± 0.06	0.6 ± 0.04
CountRecallEasy	0.39 ± 0.03	0.37 ± 0.02
CountRecallMedium	0.06 ± 0.00	0.1 ± 0.04
CountRecallHard	0.06 ± 0.01	0.05 ± 0.00
MineSweeperEasy	0.76 ± 0.01	0.73 ± 0.04
MineSweeperMedium	0.61 ± 0.02	0.59 ± 0.02
MineSweeperHard	0.55 ± 0.00	0.55 ± 0.01
NavigatorEasy	0.46 ± 0.14	0.36 ± 0.05
NavigatorMedium	-0.27 ± 0.19	-0.28 ± 0.19
NavigatorHard	-0.45 ± 0.02	-0.41 ± 0.02
NoisyCartPoleEasy	0.98 ± 0.01	0.97 ± 0.02
NoisyCartPoleMedium	0.96 ± 0.02	0.96 ± 0.01
NoisyCartPoleHard	0.92 ± 0.02	0.89 ± 0.01

Table 5: Return for the MLP model, broken down by task and observability.

Environment	MDP Return	POMDP Return
AutoEncodeEasy	0.26 ± 0.00	0.27 ± 0.00
AutoEncodeMedium	0.25 ± 0.00	0.25 ± 0.00
AutoEncodeHard	0.25 ± 0.00	0.25 ± 0.00
BattleShipEasy	0.85 ± 0.02	0.6 ± 0.04
BattleShipMedium	0.7 ± 0.04	0.56 ± 0.01
BattleShipHard	0.75 ± 0.03	0.53 ± 0.00
CartPoleEasy	0.99 ± 0.00	0.86 ± 0.02
CartPoleMedium	0.96 ± 0.01	0.47 ± 0.01
CartPoleHard	0.95 ± 0.01	0.31 ± 0.01
CountRecallEasy	0.4 ± 0.04	0.15 ± 0.01
CountRecallMedium	0.17 ± 0.02	0.06 ± 0.00
CountRecallHard	0.15 ± 0.01	0.08 ± 0.00
MineSweeperEasy	0.86 ± 0.01	0.72 ± 0.01
MineSweeperMedium	0.65 ± 0.01	0.59 ± 0.00
MineSweeperHard	0.57 ± 0.00	0.55 ± 0.00
NavigatorEasy	0.88 ± 0.02	-0.2 ± 0.05
NavigatorMedium	0.86 ± 0.01	-0.19 ± 0.02
NavigatorHard	0.94 ± 0.01	-0.07 ± 0.08
NoisyCartPoleEasy	0.94 ± 0.01	0.82 ± 0.02
NoisyCartPoleMedium	0.86 ± 0.01	0.74 ± 0.01
NoisyCartPoleHard	0.7 ± 0.01	0.66 ± 0.01

E Environment Descriptions

1. **Stateless Cartpole:** Following the classic cartpole settings from (Barto et al., 1983). Rendered with similar visualization style from (Brockman et al., 2016), but with two indicative figures to represent horizontal speed of cart and angular velocity of pole respectively.
2. **Noisy Stateless Cartpole:** Stateless Cartpole (Env. 1) affected by Gaussian noise on position and speed of the cart as well as angle and angular velocity of the pole.
3. **Battleship:** The agent’s goal is to sink all the pre-placed ships to win the game. The agent controls a cursor that represents its current position on the grid. Each turn, the agent can either move the cursor one space or choose to "FIRE" the current grid cell. Each cell can be in one of two states: HIT or MISS. The agent receives a positive reward for hitting a ship, a neutral reward (0) for the first miss on an empty cell, and a negative reward for repeatedly firing a cell that has already been targeted.
4. **Count Recall:** Every turn, the agent gets a value card and a query card. The agent’s task is to figure out how many times the query card has shown up so far. To do this, the agent counts how many times it has received the matching value card and uses that as the answer. If the agent guesses the correct count, it receives a positive reward. If the guess is incorrect, the agent receives no reward (0). This setup encourages the agent to accurately track and recall the frequency of specific cards over time.
5. **Mine Sweeper:** The agent’s goal is to hit all the non-mine cells to win the game, inspired by the classic computer game Minesweeper. Similar to Battleship environments, the agent controls a cursor to navigate the grid and can either move to an adjacent cell or "hit" the current cell each turn. Hitting a safe cell earns the agent a positive reward, while hitting a mine results in no reward (0) and ends the game. If the agent tries to hit a cell that has already been revealed, it receives a negative reward. This reward structure encourages the agent to explore efficiently, avoid mines, and minimize redundant actions to maximize its cumulative reward.
6. **Autoencode:** This game is similar to Simon but played in reverse. The agent’s task is to recall and replay a sequence of cards in the opposite order they were shown. During the WATCH phase, the agent observes a randomly generated sequence of cards. In the PLAY phase, the agent must reproduce the sequence in reverse order. The agent receives a positive reward for each correct card played and no reward (0) for incorrect choices. This environment tests the agent’s ability to encode a series of observations into a latent state and then decode that state step by step to reproduce the sequence accurately.
7. **Navigator:** The agent’s goal is to locate and confirm the treasure on the board while avoiding the TNT to win the game. The agent navigates using a cursor that marks its current position. On each turn, it can either shift the cursor to an adjacent cell or decide to confirm the cell it’s currently on. Every move the agent makes results in a small negative reward. If the agent lands on a TNT cell, it receives a significant negative reward, and the game ends immediately. This environment challenges the agent to discover the most efficient path to the treasure, aiming to maximize its cumulative reward by completing the game as quickly as possible.

F Vectorized Rendering Details

Our rendering system is built on a canvas framework. We draw to the canvas using primitives, such as letters, numbers, shapes, and more. All rendering functions are pure (without side effects), and may be easily vectorized or compiled. We build our rendering framework on top of `jax.numpy` and does not use any external dependencies. With these tools, anyone can easily render their own custom grid-based or card-based environments for further research and exploration.

Five of seven of our proposed environments come with fairly intricate rules, requiring multiple iterations of pattern rendering on the canvas. These complex tasks can be broadly split into two rendering categories: grid-based environments, like Battleship, and card-based environments, like CountRecall. Initially, we re-rendered at each step, but this was slow, even with JIT compilation. We found that removing dynamic computations improved performance, which we detail below.

Grid-based environment In grid-based games, we divide the entire canvas into a bunch of small square cells, where each cell displays either the same or a unique pattern to reflect the environmental info contained in the current state. We precompute the coordinates of every cell that needs to be drawn on the canvas and stash them in two matrices – one for the x-axis positions and one for the y-axis. During rendering, we leverage `jax.vmap` to handle the process in parallel along the row dimension.

Card-based environment We precompute all possible card templates (value, query, and historical cards) during initialization period, avoiding repetitive redrawing of static elements like suits or card positions. This turns dynamic rendering into a fast lookup-and-merge process. For example, when rendering value or query cards, we retrieve pre-drawn templates and apply them to the canvas using masks, skipping pixel-by-pixel logic during runtime. For the history display, we vectorize the drawing of historical cards using `jax.vmap`, generating all variations upfront and later selecting only the visible ones with fast array indexing. By JIT-compiling the render function, we lock these optimizations into a highly efficient, hardware-accelerated pipeline. The benefits are reduced per-frame computation, minimal branching, and GPU-friendly operations—all critical for real-time rendering. Even when rendering complex elements like the history grid, we avoid loops and instead use clever indexing with `jnp.argmax` and masks to overlay the latest valid symbols.

G Network Architecture

PQN Our Q-network combines spatial feature extraction with decision policy learning through a JAX/Equinox implementation. The network processes batches of 128×128 RGB images through four convolutional blocks, followed by three dense layers with intermediate normalization (Table 6).

Table 6: Q network architecture

Layer	Parameters	Activation
Conv2D-1	Channels: 3, 64, Kernel: 5×5 , Stride: 2	LeakyReLU
MaxPool2D-1	Pool: 2×2 , Stride: 2	–
Conv2D-2	Channels: 64, 128, Kernel: 3×3 , Stride: 2	LeakyReLU
MaxPool2D-2	Pool: 2×2 , Stride: 2	–
Conv2D-3	Channels: 128, 256, Kernel: 3×3 , Stride: 2	LeakyReLU
MaxPool2D-3	Pool: 2×2 , Stride: 2	–
Conv2D-4	Channels: 256, 512, Kernel: 1×1 , Stride: 1	LeakyReLU
Dense-1	Features: 512, 256	LeakyReLU
LayerNorm	Shape: 256	–
Dense-2	Features: 256, 256	LeakyReLU
LayerNorm	Shape: 256	–
Dense-3	Features: 256, 5	–

PQN \times RNN Our recurrent Q-network extends the base architecture with explicit memory handling through a hybrid CNN-RNN-MLP design. The RNN combines a 512-channel input tensor x with a 5-dimensional one-hot encoded last action vector from POPGym Arcade, processes these through its 512-unit hidden state, and generates 256-dimensional output features (Table 7).

Table 7: Recurrent Q network architecture

Layer	Parameters	Activation
Conv2D-1	Channels: 3, 64, Kernel: 5×5 , Stride: 2	LeakyReLU
MaxPool2D-1	Pool: 2×2 , Stride: 2	–
Conv2D-2	Channels: 64, 128, Kernel: 3×3 , Stride: 2	LeakyReLU
MaxPool2D-2	Pool: 2×2 , Stride: 2	–
Conv2D-3	Channels: 128, 256, Kernel: 3×3 , Stride: 2	LeakyReLU
MaxPool2D-3	Pool: 2×2 , Stride: 2	–
Conv2D-4	Channels: 256, 512, Kernel: 1×1 , Stride: 1	LeakyReLU
RNN Cell	Input, Hidden, Output: 517, 512, 256, Num Layer: 2	
Dense	Features: 256, 5	–

H Recurrent Models

In this section, we describe all recurrent models used in our work.

Linear Transformers Standard transformers have quadratic space complexity from the outer product of keys and queries. The Fast Autoregressive Transformer (FART) (Katharopoulos et al., 2020) replaces softmax attention with a kernelized attention mechanism to achieve linear space complexity and logarithmic time complexity via associative recurrent updates

$$h_t = h_{t-1} + \phi(W_k x_t) \phi(W_v x_t)^\top \quad \hat{s}_t = \text{MLP} \left(x + \frac{\phi(W_q x_t)^\top h_t}{\phi(W_q x_t) \cdot \sum_{i=0}^t \phi(W_k x_i)} \right). \quad (10)$$

Here, $\phi(x) = 1 + \text{ELU}(x)$ represents a kernel-space projection and the recurrent state h represents the attention matrix. W_k, W_v, W_q represent the key, query, and value projection parameters. To compute \hat{s}_t , we multiply the recurrent attention matrix by the query vector and normalize by a scalar.

State-Space Models State-Space Models (SSMs) (Gu et al., 2022) model an associative recurrence via

$$h_t = \overline{W}_A h_{t-1} + \overline{W}_B x_t \quad \hat{s}_t = \overline{W}_C h_t + \overline{W}_D x_t, \quad (11)$$

where $\overline{W}_A, \overline{W}_B, \overline{W}_C, \overline{W}_D$ are discretizations of carefully initialized trainable parameters W_A, W_B, W_C, W_D . In practice, we initialize W_A, W_B, W_C, W_D deterministically. Deterministic initialization applied to many consecutive SSM layers can result in instabilities, and so Orvieto et al. (2023) proposes a meticulously derived random initialization and new parameterization of SSM parameters. They call their method the Linear Recurrent Unit (LRU).

Minimal Recurrent Networks Feng et al. (2024) revisit the popular Gated Recurrent Unit (GRU) (Chung et al., 2014) and Long Short-Term Memory (LSTM) (Hochreiter & Schmidhuber, 1997) RNNs. They simplify the GRU and LSTM recurrent updates, proposing the MinGRU and MinLSTM with efficient associative recurrent updates. The authors write the MinGRU as

$$h_t = (1 - \sigma(W_1 x_t + b_1)) \odot h_{t-1} + \sigma(W_1 x_t + b_1) \odot \tanh(W_2 x_t + b_2) \quad \hat{s}_t = h_t, \quad (12)$$

with trainable parameters W_1, b_1, W_2, b_2 , sigmoid function σ , and elementwise product \odot . The authors find that the MinGRU outperforms multiple SSM variants across offline reinforcement learning tasks, using an offline decision transformer (Chen et al., 2021) framework.

I Experiment Hyperparameters

Experiment hyperparameters were taken from the original PQN paper (Gallici et al., 2024). We slightly modified the hyperparameters to minimize training time and produce more stable return curves.

Table 8: PQN hyperparameters used in all of our experiments. See Gallici et al. (2024) for a detailed description of hyperparameters.

Parameter	Value
TOTAL_TIMESTEPS	10e6,20e6,100e6
TOTAL_TIMESTEPS_DECAY	1e6,2e6,20e6
NUM_ENVS	16
MEMORY_WINDOW	4
NUM_STEPS	128
EPS_START	1.0
EPS_FINISH	0.05
EPS_DECAY	0.25
NUM_MINIBATCHES	16
NUM_EPOCHS	4
NORM_INPUT	False
NORM_TYPE	layer norm
LR	0.00005
MAX_GRAD_NORM	0.5
LR_LINEAR_DECAY	True
REW_SCALE	1.0
GAMMA	0.99
LAMBDA	0.95

J Compute Resources

We used approximately 98 days equivalent training time on an RTX4090 GPU to produce a little over 1,000 total runs. We used an unknown amount of additional resources to tune hyperparameters and rerun experiments after fixing bugs.